Spread spectrum-based ultraviolet communication with experiments

Min Zhang (张 民)*, Pengfei Luo (罗鹏飞), Xiaoxue Guo (郭晓雪), Xiang Zhang (张 翔), Dahai Han (韩大海), and Qing Li (李 青)

State Key Laboratory of Information Photonics and Optical Communications, Beijing University of Posts and Telecommunications, Beijing 100876, China

**Corresponding author: mzhang@bupt.edu.cn*

Received March 3, 2014; accepted July 3, 2014; posted online September 11, 2014

We report experiments of ultraviolet (UV) communication based on spread-spectrum technique. Field measurements via online UV communication are conducted to compare the system performances with and without spectrum spreading. The results indicate that the spread-spectrum technique is capable of suppressing noise in UV atmospheric scattering channel and therefore improve the system performance evidently. Details of implementation are also provided to make the results useful for similar system design in research on optical wireless communications.

OCIS codes: 060.2605, 060.4510.
doi: 10.3788/COL201412.100602.

Ultraviolet (UV) light has gained much research attention owing to its unique characteristics[1,2]. Atmospheric scattering of UV radiation makes it a possible candidate for short-range light-of-sight (LOS) and, to some extent, non-LOS (NLOS) communication[3,4] and relevant experiments have been conducted[5–8]. However, the performance of UV communication suffers from unfavorable open environment due to solar background noise, climate conditions, interference from the other UV sources, and so on[9,10]. In recent years, schemes have been reported to improve UV communication systems, by using moving average filter, spectral amplitude coding, spatial diversity reception, and so on[11–14].

Spread-spectrum technique, combined with broadband transmission and correlation reception, possesses the ability of anti-jamming and anti-multipath fading in wireless communications at traditional frequencies. Spread-spectrum-based infrared (IR) communication has been presented by O'Farrell *et al.*[15–18]. In their experiments, an IR signal at 850 nm, at 1 or 2 Mbps, was spectrum spread through direct-sequence spread spectrum (DSSS). With the total optical power of 6 mW from IR light-emitting diodes (LEDs), the receiver responsibility of about –42 dBm and given bit error rate (BER) $< 10^{-5}$, the LOS communication distance was within 2–4 m. Accordingly, O'Farrell *et al.* tended to apply their proposed system mainly in indoor LOS communication. However, UV communication based on spread-spectrum technique has not been reported till now. The UV light, at frequencies of 10^{14}–10^{16} Hz, exhibits more particle-like characteristic in its wave-particle duality. The validity of spread-spectrum technique in improving UV communication is not reported theoretically or experimentally.

Here we design and implement an UV communication system with spread-spectrum technique. Our main contribution lies in the fact that to the best of our knowledge this is the first report of spread-spectrum-based UV communication system, and the feasibility of spread-spectrum technique in improving the UV communication is verified through online UV communication experiments with various receiver elevations and distances. In addition, details of implementation and performance comparison are provided to make the results useful for similar system design in research on optical wireless communications.

The noise in UV channel is mainly the band-limited noise, but strictly it is not band-limited additive white Gaussian noise[12]. Besides narrowband noise, broadband noise also exists in UV channel. For the narrowband noise in UV channel, after spectrum spreading and correlation reception, its spectrum is broadened and lowered. By applying narrowband filtering, only a little narrowband noise will interfere with the effective signal. For the broadband noise, its spectrum will not be compressed after correlation reception, whereas the signal spectrum is compressed evidently, since the de-spreading code for the signal does not match with the random noise. Therefore, only a small part of broadband noise will exist within the compressed signal spectrum.

The improvement by spread-spectrum technique can be roughly revealed by the correlation gain G[19]:

$$G = \frac{W}{\Delta F}, \tag{1}$$

where ΔF and W are the bandwidths before and after spectrum spreading, respectively.

Here we adopt the simple DSSS technique for UV communication. The pseudorandom binary sequences (PRBSs) used for DSSS include mainly M-sequence, gold code, JPL code, and so on. Gold code-based DSSS claims higher performance at the cost of higher complexity. JPL code-based DSSS enables faster capture,

but with higher complexity too. M-sequence-based DSSS is of moderate performance but easy to implement. Here we select the simple M-sequence to test the improvement by DSSS to UV communications, and in its implementation we apply the sequence inversion keying (SIK) for the following reasons. Firstly, SIK with equal numbers of "1" and "0", has no DC component and thus is favorite to the power limited UV LED. Secondly, since SIK is a balanced code, the data can be detected via a zero threshold, which is insensitive to the variation of the channel properties and thus improve the anti-noise performance. In short, SIK possesses the advantages of bipolar code which is much easier for implementation[20,21].

For example, let us take SIK-7. The original on-off keying (OOK) signal and the corresponding SIK-7 signal, seven times of its original frequency are shown in Fig. 1. Each "1" bit of the OOK signal is coded as PRBS1 "1110010", whereas each "0" bit is coded as PRBS0 "0001101". Here, PRBS1 and PRBS0 are complement forms to each other. The frequency of SIK-7 is seven times that of OOK signal. Then the gain G in Eq. (1) is roughly 7.

We apply the majority logic judgment in de-spreading for its simple and reliable characteristics[22,23]. At the receiver side, after synchronization, we take XOR between every received 7 bits of the SIK-7 signal and PRBS1 and then the seven XOR results are summed up. If the sum is less than $G/2$, we judge it as "1" and otherwise it is "0". After de-spreading, the error rate Pe is approximated as[18]:

$$P_e = \sum_{k=(G+1)/2}^{G} C_G^k p^k (1-p)^{(G-k)}, \tag{2}$$

where p is the chip error rate (CER) after the majority logic judgment.

Equation (2) indicates that the received signal can be recovered correctly as long as the error codes are less than 50%. We plot the relationship between CER at the receiver and BER after spread spectrum. As shown in Fig. 2, the spread-spectrum technique may drop the BER significantly, and moreover larger G or higher order SIK leads to lower BER in principle. As an example, if a signal is detected with a CER of 10^{-5}, the BERs after de-spreading for $G = 7$ is predicted to be reduced to 10^{-20}.

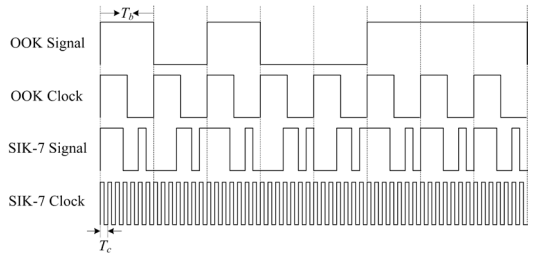

Fig. 1. Original OOK signal and the corresponding SIK-7 signal.

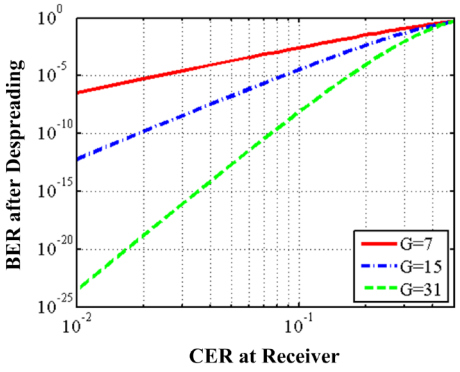

Fig. 2. Relationship between CER at the receiver and BER after de-spreading.

To predict the improvement for UV communication specifically, we conduct theoretical analysis and simulation. At the transmitter, we take SIK to a non-return-to-zero (NRZ) signal $b(t)$ with a pulse period of T_b, namely,

$$b(t) = \sum_{k=-\infty}^{\infty} b_k g(t - kT_b), \tag{3}$$

where $g(t)$ is a normalized window function with a width of T_b and $b_k \in \{0, 1\}$ is the value of the kth bit.

The chip for SIK is a NRZ m-sequence $c(t)$ with a period of T_c, namely

$$c(t) = \sum_{j=-\infty}^{\infty} c_j g_c(t - jT_c), \tag{4}$$

where $g_c(t)$ is a normalized window function for the chip, its width is T_c, and $c_j \in \{0, 1\}$ is the value of the jth bit.

Therefore, after spectrum spreading, the signal can be expressed as

$$s(t) = b(t) \oplus c(t). \tag{5}$$

With the consideration of the scattering-induced multipath effect, we express the transfer function of the UV channel as

$$h(t) = \sum_{i=0}^{L-1} \beta_i \delta(t - \tau_i), \tag{6}$$

where L is the total number of the resolved multipaths, τ_i is the time delay of the ith resolved multipath, and β_i is its normalized amplitude determined by the scattering and the environment. For calculation of β_i, we trace every photon packet's initialization, random interaction distance, random migration direction, absorption probability, and detection probability after each scattering event. Then we use a statistical model, namely Monte Carlo algorithm, to obtain the path loss and the channel impulse response by simulating a large number of photons[24].

At the receiver, the detected signal $r(t)$ is presented as

$$\begin{aligned} r(t) &= \int_{-\infty}^{\infty} R \cdot s(\tau) \cdot h(t - \tau) \mathrm{d}\tau + n(t) \\ &= \sum_{i=0}^{L-1} R P_{\mathrm{av}} \beta_i s(t - \tau_i) + n(t), \end{aligned} \tag{7}$$

where R is the photoelectric conversion efficiency of photomultiplier tube (PMT), $n(t)$ is the noise, and P_{av}

is the average power of the optical signal at the receiver.

After synchronization, taking the correlation between $r(t)$ and $c(t)$, we get

$$y(t) = \frac{1}{T_b}\int_0^{T_b} r(t)c(t)\mathrm{d}t = B(t) + N(t), \tag{8}$$

which means the output is a combination of the de-spreading signal $B(t)$ and a comprehensive noise $N(t)$. The original bit sequence $\{b_k\}$ is obtained by integrating $B(t)$ over each shifted bit duration T_b and then sampling, whereas the noise contains three parts, namely

$$N = \frac{n_{\mathrm{BG}}}{G} + n_{\mathrm{PMT}} + n_{\mathrm{ISI}}, \tag{9}$$

where n_{BG}/G represents the compressed background noise. G is the correlation gain given in Eq. (1) and it is actually T_b/T_c in SIK case. In calculation, we approximate n_{BG} as a narrowband additive noise. According to the measured background noise of UV channel in daylight[12], we apply a fitting function for it as a weighted sum of a Gaussian function and a Chi-squared distribution.

In Eq. (9), n_{PMT} is for the noise introduced from the UV PMT and the amplification circuit. In calculation, we take into consideration of the photon noise, the photocathode noise, and the thermal noise, because they have relatively high amplitudes and meanwhile are sensitive to the signal frequency.

In Eq. (9), n_{ISI} is the inter-symbol interference (ISI) induced by the multipath effect, the phase asynchronization, and the sampling error. Here n_{ISI} is expressed as[17,18]

$$n_{\mathrm{ISI}} = \frac{RP_{\mathrm{av}}}{G}\sum_{i=1}^{L-1}\beta_i\left[b_{-1}C_c(l-G) + b_0C_c(l)\right], \tag{10}$$

where $C_c(l)$ is a periodic autocorrelation function (ACF) of the spreading sequence and its period is just G.

It is noted from Eqs. (9) and (10) that, by using an m-sequence as the SIK sequence, both the noises n_{BG} and n_{ISI} are reduced by a factor of G.

By taking $B(t)/N(t)$ as the signal-to-noise ratio (SNR), we can estimate the BER after de-spreading as

$$\mathrm{BER} = Q(\sqrt{\mathrm{SNR}}). \tag{11}$$

The resulting BER for LOS UV communication is shown in Fig. 3, where the LED output power is 1.6 mW at 265 nm and the divergence angle is 10°. The original signal is a repeated PRBS with the length of 2^{15}-1 at 8 kbps. At the receiver, a PMT is taken as the detector of which the field of view (FOV) is 30°. Its cathode sensitivity R and quantum efficiency η are set as 62 mA/W and 30%, respectively.

It is observed from Fig. 3 that the BER performance is improved obviously after SIK-based spectrum spreading. Particularly, within shorter distance, for example, 10–15 m, the BER for SIK is reduced by a factor of 100. As distance increases, the BER improvement tends

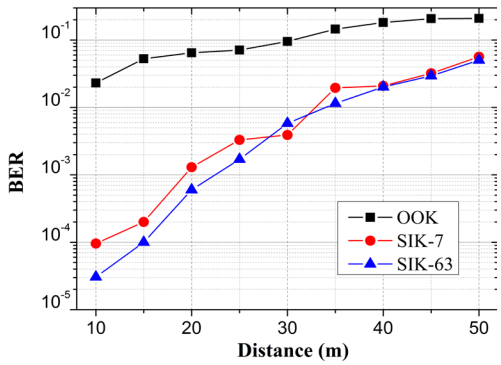

Fig. 3. Simulated BER after de-spreading for LOS UV communication.

to be leveled due to a dramatically degraded SNR, and meanwhile, the difference between SIK-7 and SIK-63 becomes negligible, which means that the simple but effective SIK-7 is preferable in practice. Even within shorter distance, the BER performance of SIK-63 is only slightly better than that of SIK-7, which is different from the numerical estimation in Fig. 2 that higher order SIK means higher correlation gain G and leads to lower BER. The reason may be that the frequency selective fading of the UV channel dominates in its multipath effect and thus signal at higher frequency suffers more from cross modulation. The second reason is that the main noise factors at the receiver, especially the photon noise and the photocathode noise are almost proportional to the signal frequency.

In comparison with SIK-based IR communication, we have estimated the performance of SIK-based UV communication with higher power and bitrate according to the measured background noise and the path loss. Given the optical power of 10 mW, the OOK bitrate of 1 Mbps, and transmitter/receiver elevations of (30°, 0°), the UV NLOS communication span with SIK-7 is simulated to be 30 m in daylight.

The experimental system is designed as shown in Fig. 4. The transmitter consists of a data source, field-programmable gate array (FPGA) module to perform

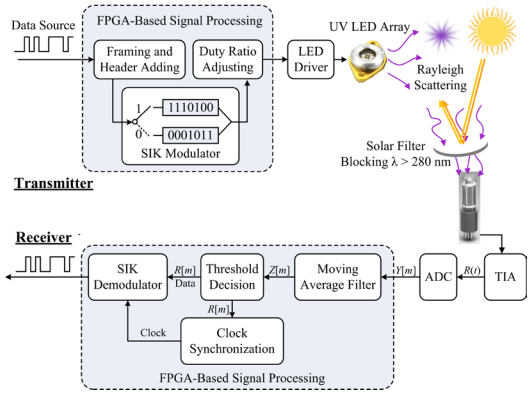

Fig. 4. Structure of the experimental system of spread-spectrum-based UV communication.

header adding, framing, and SIK-based spectrum spreading, and an UV LED array with driver circuit. The receiver is mainly composed of a PMT with a low-noise transimpedance amplifier (TIA), an analog-to-digital converter (ADC), a FPGA module for synchronization, digital filtering, spectrum de-spreading, and BER analyzing.

We adopted a simple DSSS method, namely SIK, in spectrum spreading and applied the majority logic judgment in de-spreading. To illustrate the implementations of the DSSS modulation and demodulation, we take SIK-7 for example. In SIK-7 modulation, the original OOK signal is converted into bit sequence seven times its original frequency. In SIK-7 demodulation, every received seven chips are grouped into a code block. Each code block is taken into the correlation with PRBS "1110010" and its complement "0001101". Then two new 7-bit code blocks are resulted, by comparing which we can decide whether the restored signal is "1" or "0".

The FPGA-based block diagram for SIK modulation is shown in Fig. 5, which consists of five modules: clock module provides programmable frequency divider; control module performs initialization, enabling, and reset; DSSS module realizes the SIK-based spectrum spreading; string conversion module converts the parallel spread signal to serial bit stream for sending; duty ratio adjusting module adjusts the pulse width since the lifetime of the UV LED is limited. Through the DSSS modulation, the original OOK signal is converted into bit sequence at n times of its original frequency if SIK-n is used, as exemplified by the SIK-7 signal as shown in Fig. 4.

The FPGA-based block diagram for SIK demodulation is shown in Fig. 6, where storage module catches the received spread signal and recovers the duty cycle; synchronous clock extraction module performs clock synchronizing; demodulation module de-spreads the received signal according to PRBS correlation[22]; BER module is a programmable BER analyzer; serial port module yields the original signal to sink.

The flow chart of the SIK demodulation procedure is shown in Fig. 7. After bit synchronization and phase

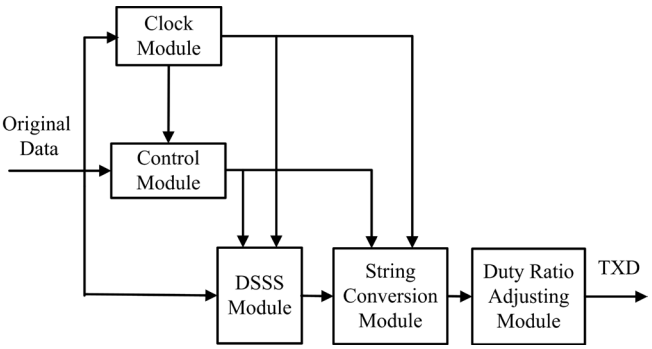

Fig. 5. FPGA-based block diagram for SIK modulation.

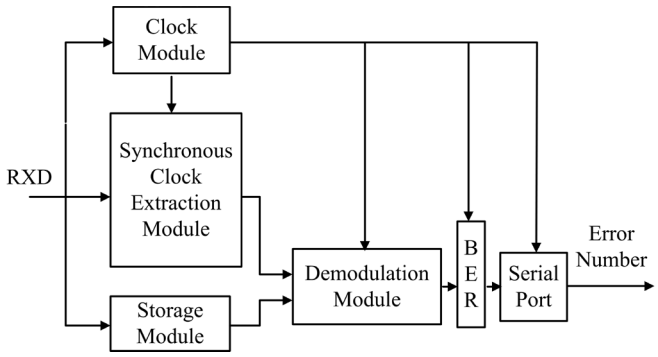

Fig. 6. FPGA-based block diagram for SIK demodulation.

synchronization, every received seven chips are grouped into a code block. Then each code block is taken into the correlation with PRBS "1110010" and its complement "0001101". Thus we get two new 7-bit code blocks and store them in two registers named as *data* and *data_r*. The numbers of "1" in *data* and *data_r* are counted and named as *Num* and *Num_r*. By comparing *Num* and *Num_r*, we can decide whether the restored signal is "1" or "0". If $Num \geq Num\_r$, the corresponding code block stands for "1". Otherwise, it stands for "0". The recovered bit sequence is then stored in a register named as *data_out* and BER is calculated.

We proposed and implemented a simple but effective algorithm to ensure the accuracy of phase synchroniza-

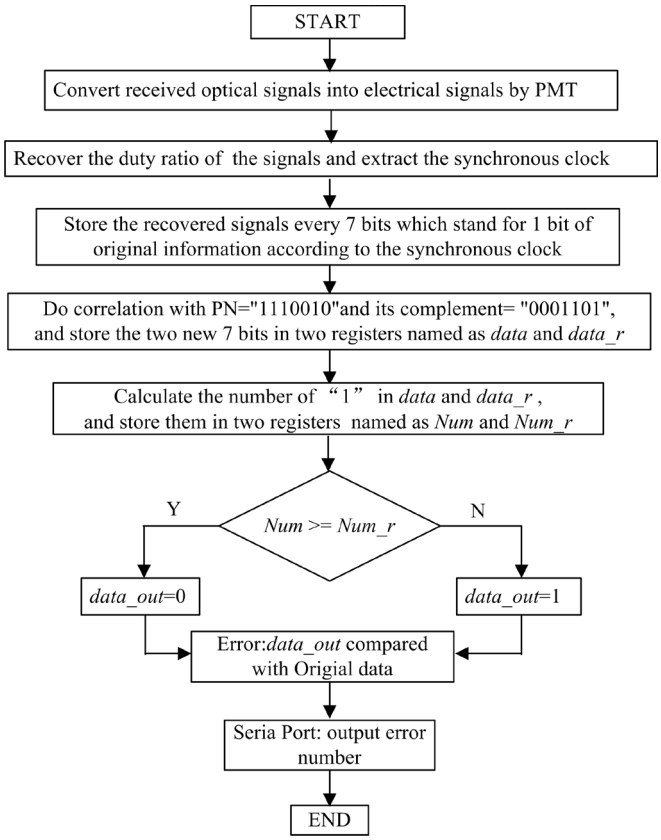

Fig. 7. Flow chart of the SIK demodulation procedure.

tion, as it affects the system performance directly[23]. Firstly, we encapsulate every received P bits into a frame and then add a Q-bit header to each frame. In each header, the first Q-2 bits are "1"s serving as the synchronization sequence and the last 2 bits are "0"s serving as the start delimiter. The phase synchronization procedure consist of two steps: (1) extract the correlation peaks by preprocessing and (2) determine the PRBS phase.

The block diagram of preprocessing is shown in Fig. 8. The correlator calculates the correlation between the PRBS $X[m]$ and $R[m]$, where $R[m]$ is the received signal from ADC. The output $P_{\mathrm{RX}}[m]$ is calculated as

$$P_{\mathrm{RX}}[m] = \sum_{n=1}^{N} R[n+m]X^{*}[n]. \tag{12}$$

After the threshold decision, a string $S_{\mathrm{P}}[m]$ is yielded, in which each "1" presents a pulse exceeding the threshold in $P_{\mathrm{RX}}[m]$.

Since the position of "1" in $P_{\mathrm{RX}}[m]$ appears irregularly as CER increases, further processing is needed, of which the block diagram is shown in Fig. 9, where $S_{\mathrm{P}}[m]$ is converted to $P_{\mathrm{P}}[m]$ via a series shift additions and then the peaks in $P_{\mathrm{P}}[m]$ are picked and identified.

In the series shift additions, $S_{\mathrm{P}}[m]$ is shifted by T_{b} each time and it is totally shifted Q-3 times, yielding Q-2 code groups. For SIK-7 de-spreading, taking the last 7 bits in original $S_{\mathrm{P}}[m]$ as the reference positions, we calculate the sum of "1"s in each of these positions in the Q-2 code groups and thus get seven numbers to construct $S_{\mathrm{P}}[m]$. Searching for the maximum value of $S_{\mathrm{P}}[m]$, we identify the correct phase for SIK-7 de-spreading.

We conducted experiments to evaluate the system performance with and without spread-spectrum technique. The system structure is shown in Fig. 4 and the established system is shown in Fig. 10.

At the transmitter, an UV LED array (UV-CLEAN265HS-10, SETi) was applied, for which the maximum output power was 10 mW at 265 nm and the divergence angle was 10°. However, in our experiments, the communication span was within 20 m and in order to evaluate the BER performance of DSSS-based UV communication, we had to reduce the LED output power as 1.6 mW. In fact, we conducted experiments

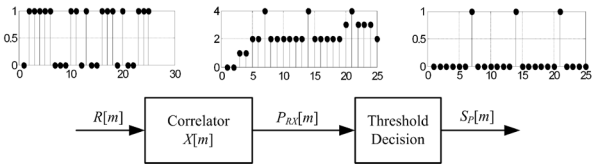

Fig. 8. Block diagram of preprocessing in phase synchronization.

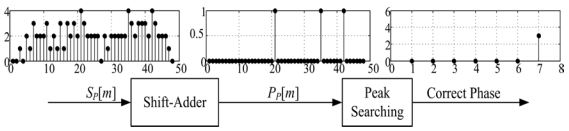

Fig. 9. Block diagram of determination in phase synchronization of PRBS.

with higher UV LED powers, but there was almost no error bit detected.

At the receiver, a PMT (R7154, Hamamatsu) was employed as the detector, of which the FOV was 30° and the maximum gain was 10^7. In the experiments, we adjusted the gain to be around 4×10^5 via its supply voltage.

We applied a narrowband interference UV filter before the PMT to block off the UV light with wavelength longer than 280 nm. The angular transmittance of the UV filter is shown in Fig. 11. In the case of vertical incidence, the transmittance is 20% at its center wavelength 266 nm, the out-of-band attenuation is ~0.1% and the full-width at half-maximum is 15 nm.

For digital signal processing, a pair of FPGA chips (Cyclone II series, EP2C8Q208C8N, Altera) was employed. We designed the average points for the moving average filter as 8 bits. The sampling frequency of the ADC is 8 MHz and its sampling precision is 8 bits.

In the experiments, every 1000 bits of the PRBS was encapsulated as a frame, serving as the signal to be

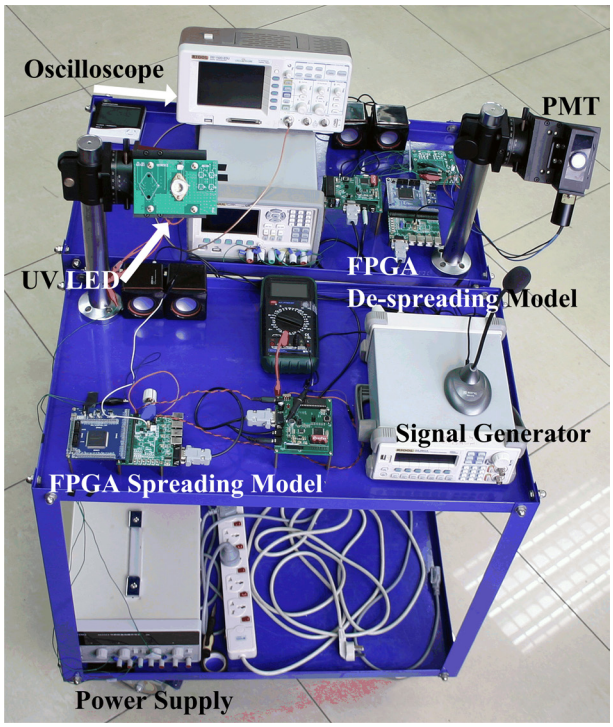

Fig. 10. Experimental system of spread-spectrum-based UV communication.

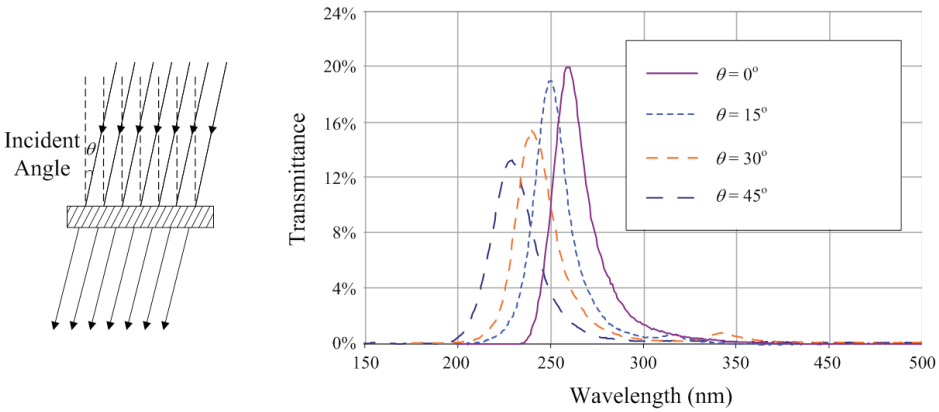

Fig. 11. Angular transmittance of the interference UV filter.

sent. The original bitrate was 8 kbps. The output from the transmitter was 56 kcps in the case of SIK-7 and 504 kcps in the case of SIK-63. For each measurement, we sent 4000 frames. Since the bit number was limited for each measurement, we defined BER = 2.5×10^{-7} instead of BER = 0 if there was no error bit at the receiver.

With the receiver elevation of 17° and the transmitter elevation of 0°, we measured and compared the BER of OOK/SIK-7/SIK-63-based UV communication at different distances. The experimental results are listed in Table 1 and plotted in Fig. 12.

Due to atmospheric scattering, the BER of OOK-based system increased as the distance increased, as shown in Fig. 12. However, with spread-spectrum technique, the BER performance was evidently improved. Specifically, the BER with SIK-7 was around 1/10 of that with OOK, and the BER with SIK-63 dropped even lower, around 1/25–1/40 of that with OOK. Therefore, the spread-spectrum technique does work in anti-noise and anti-multipath in UV atmospheric scattering channel.

We have noticed that the communication is more sensitive to the transmitter elevation but insensitive to the receiver elevation in the absence of a filter in front of the PMT[10]. However, in our experiments with a filter, the system performance became sensitive to the receiver elevation too. We fixed the transmitter elevation as 0° and the distance as 15 m, and then measured the BER after de-spreading. The experimental results are listed in Table 2 and plotted in Fig. 13.

Table 1. Measured BER of OOK/SIK-7/SIK-63 based UV Communication Systems at Different Distances

Modulation	Distance		
	5 m	**10 m**	**15 m**
OOK	4.685×10^{-2}	1.087×10^{-1}	1.907×10^{-1}
SIK-7	5.150×10^{-3}	8.031×10^{-3}	9.550×10^{-3}
SIK-63	1.800×10^{-3}	3.225×10^{-3}	4.325×10^{-3}

Firstly, we identified the obvious improvement brought by the spread-spectrum technique at various receiver elevations. Specifically, the BER with SIK-7 was around 1/10–1/320 of that with OOK. The BER with SIK-63 became even lower. Moreover, we conducted experiments when the receiver elevation was less than 10°, the BER improvement by spread-spectrum technique became very significant, in which the BERs with SIK-7 and SIK-63 approached to 0. These results show that, with spread-spectrum technique, the receiver is able to work at relaxed elevation angles and thus the flexibility of the UV communication system becomes higher. From another perspective, the spread-spectrum technique provides the UV communications system a strengthened ability of anti-multipath.

Secondly, we also observe from Fig. 13 that the system performance is sensitive to the receiver elevation with the advent of an UV filter. The reason is that the transmittance of the interference UV filter used here is sensitive to the ray incident angle, as shown in Fig. 11, which leads to FOV decreasing as the receiver elevation rises. As an alternative, an absorbing UV filter is insensitive to the ray incident angle but its transmittance is usually very low. If an absorbing UV filter

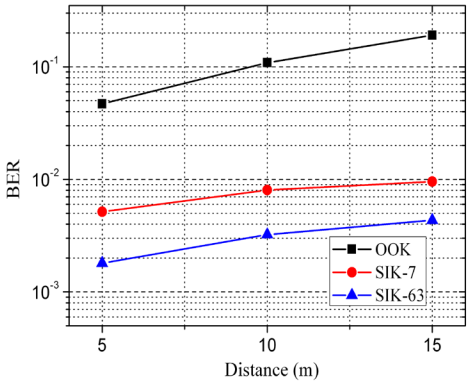

Fig. 12. Measured BER of OOK/SIK-7/SIK-63-based UV communication at different distances, with original bitrate 8 kbps, output optical power 1.6 mW at 265 nm, transmitter elevation 0°, receiver elevation 17°, and FOV 30°.

Table 2. Measured BER of OOK/SIK-7/SIK-63-based UV Communication Systems at Various Receiver Elevations

Modulation	Receiver Elevation				
	10°	12°	15°	17°	19°
OOK	3.195×10^{-2}	4.080×10^{-2}	5.628×10^{-2}	1.907×10^{-1}	3.297×10^{-1}
SIK-7	1.000×10^{-4}	1.000×10^{-3}	5.400×10^{-3}	9.550×10^{-3}	2.330×10^{-2}
SIK-63	$< 10^{-4}$	4.800×10^{-4}	2.550×10^{-3}	4.325×10^{-3}	5.500×10^{-3}

with high transmittance is available, together with the spread-spectrum technique, the UV communication will become more flexible.

In conclusion, we theoretically analyze the performance of UV communication with spread-spectrum technique, and implement such a system. We conduct experiments of SIK-based UV communication and compare the system performances with and without SIK. The results show that the spread-spectrum technique is able to improve the performance of UV communication system evidently, and the improvement is more significant in the case of LOS communication. Besides, results of both simulations and experiments show that BER performance for SIK-63 is only slightly better than SIK-7, which means that the frequency selective fading may dominate over the time selective fading in UV multipath effect, and also simple but effective SIK-7 is preferable in practical UV communication. Finally, estimation of the system performance with higher power and bitrate indicates that the SIK-based UV communication is possible to be applied in outdoor quasi-LOS and even NLOS scenarios.

This work was supported by the National Natural Foundation of China(No. 61101110) and the Doctoral Scientific Fund of Ministry of Education of China (No. 20120005110010).

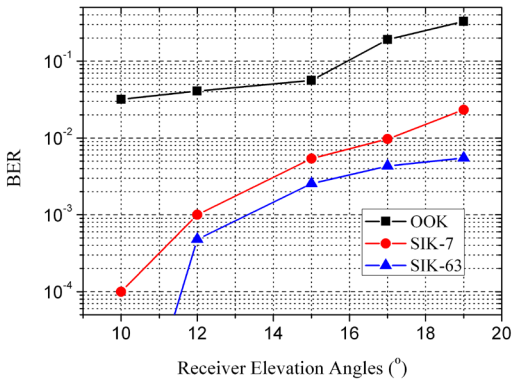

Fig. 13. Measured BER of OOK/SIK-7/SIK-63-based UV communication at various receiver elevations, with original bitrate 8 kbps, output optical power 1.6 mW at 265 nm, transmitter elevation 0°, and distance 15 m.

References

1. Y. Peng, Z. Fang, and E. Zang, Chin. Opt. Lett. **10,** S11405 (2012).
2. J. Zhang, Y. Yang, and H. Jia, Chin. Opt. Lett. **11,** 102304 (2013).
3. G. L. Harvey, "A survey of ultraviolet communication systems" Naval Research Laboratory Technical Report (1964).
4. Z. Y. Xu and B. M. Sadler, IEEE Commun. Mag. **46,** 67 (2008).
5. W. S. Ross and R. S. Kennedy, "An investigation of atmospheric optically scattered non-line-of-sight communication links" Army Research Office Project Report (1980).
6. J. J. Puschell and R. Bayse, in *Proceedings of the Tactical Communications* 253 (1990).
7. Q. He, Z. Xu, and B. M. Sadler, Opt. Express **18,** 12226 (2010).
8. H. Zhang, H. Yin, H. Jia, J. Yang, and S. Chang, Opt. Express **19,** 21216 (2011).
9. Z. Y. Xu, H. P. Ding, B. M. Sadler, and G. Chen, Opt. Lett. **33,** 1860 (2008).
10. P. Luo, M. Zhang, and D. Han, Opt. Express **20,** 23489 (2012).
11. H. F. Xiao, Y. Zuo, J. Wu, Y. Yan, and J. T. Lin, Opt. Lett. **37,** 4143 (2012).
12. P. Luo, M. Zhang, Y. Liu, and D. Han, in *Proceedings of IEEE CSNDSP* 18 (2012).
13. M. Noshad and M. Brandt-Pearce, in *Proceedings of GLOBECOM* 843 (2011).
14. D. Han, Y. Liu, K. Zhang, P. Luo, and M. Zhang, Opt. Express **20,** 15833 (2012).
15. T. O'Farrell and M. Kiatweerasakul, in *Proceedings of IEEE 5th International Symposium on Spread Spectrum Techniques and Applications* 752 (1998).
16. T. O'Farrell and M. Kiatweerasakul, in *Proceedings of IEEE 9th International Symposium on Personal, Indoor and Mobile Communications* 703 (1998).
17. K. K. Wong, T. O'Farrell, and M. Kiatweerasakul, Int. J. Commun. Syst. **13,** 511 (2000).
18. K. K. Wong and T. O'Farrell, IEEE Wireless Commun. **10,** 54 (2003).
19. R. L. Pickholtz, L. B. Milstein, and D. L. Schilling, IEEE Trans. Vehicular Technol. **40,** 313 (1991).
20. T. O'Farrell and S. Lochmann, Electron. Lett. **30,** 63 (1994).
21. M. L. Pham, K. Makelainen, and A. B. Sharma, in *Proceedings of International Conference on Communication Technology* (ICCT) 567 (1996).
22. C. C. Kilgus, IEEE Commun. Trans. **21,** 772 (1973).
23. J. H. Lee, I. Song, S. R. Park, and J. Lee, IEEE Trans. Vehicular Technol. **53,** 49 (2004).
24. H. Ding, G. Chen, A. K. Majumdar, B. M. Sadler, and Z. Xu, IEEE J. Sel. Areas Commun. **27**, 1535 (2009).